Available online at www.sciencedirect.com
SCIENCE DIRECT®
Journal of Solid State Chemistry 176 (2003) 97–104
JOURNAL OF SOLID STATE CHEMISTRY
http://elsevier.com/locate/jssc

# Phase transitions in the perovskite methylammonium lead bromide, $CH_3ND_3PbBr_3$

I.P. Swainson,[a,*] R.P. Hammond,[a] C. Soullière,[a] O. Knop,[b] and W. Massa[c]

[a] *Neutron Program for Materials Research, National Research Council, Chalk River Laboratories, Stn. 18, Chalk River, Ont., Canada K0J 1J0*
[b] *Department of Chemistry, Dalhousie University, Halifax, NS, Canada B3H 4J3*
[c] *Department of Chemistry, Philipps University, D-35032 Marburg, Germany*

Received 17 December 2002; received in revised form 24 June 2003; accepted 28 June 2003

**Abstract**

The structure of phase IV of methylammonium lead bromide, $CH_3ND_3PbBr_3$, is shown from Rietveld refinement of neutron powder diffraction data to be centrosymmetric, with space group *Pnma*: $Z = 4$; $a = 7.9434(4)$ Å, $b = 11.8499(5)$ Å, $c = 8.5918(4)$ Å at 11 K; $R_{wp} = 2.34\%$ $R_p = 1.81\%$. This corresponds to one of the pure tilt transitions, $a^-b^+a^-$, commonly observed in perovskites. Additional distortions not required by pure tilting are found in the $PbBr_6$ octahedra, and it appears that the structure optimizes the hydrogen bonding between the methylammonium cation and the framework. It is likely that the lowest temperature phase of the corresponding iodide also has this structure. The structure is compared to the available data for that of other *Pnma* perovskites. A brief comparison to the higher temperature phases in which the methylammonium ion is disordered is given.


*Keywords:* Methylammonium lead halides; Perovskites; Hydrogen-bonding; Order–disorder; Rietveld refinement; Neutron powder diffraction

## 1. Introduction

The methylammonium lead halides (MAPX) are an interesting group of compounds that crystallize as perovskites. Perovskites have the general formula $ABX_3$, where $A$ is usually a large cation, often an alkali, and $B$ a metal octahedrally coordinated by an anion $X$. Perovskites have been the subject of great interest for many years, due to the large number of compounds which crystallize in this structure, the novel properties of certain perovskites, and the large number of phase transitions found in these systems.

One set of these transitions, often termed tilting transitions, is due to the corner connectivity of all the octahedra. The situation is similar to the corner-bonded frameworks of tetrahedra in which there are many such transitions due to the presence of low-frequency phonons (Rigid Unit Modes, RUMs) that do not distort the main structural units (tetrahedra) of the framework [1,2]. Hammonds et al. [2] showed that a line of such zero-frequency phonons exist along the $R$–$M$ zone boundary of idealized cubic perovskites. Nevertheless, it appears that the general result is that there are far fewer such RUMs in frameworks containing corner-bonded octahedra. This is because of the higher degree of constraint (number of corners per polyatomic unit) in such systems. Only in octahedral systems such as perovskite, in which the aristotype has very high symmetry, and in which many of the constraints become degenerate, will there be any appreciable number of RUMs.

One early systematic view of the transitions in perovskites was that of Glazer [3,4] who examined the problem in direct space, deduced possible tilt systems, and introduced a notation for describing them. Recently, two new systematic attempts have been made using group analysis to determine possible representations for transitions and the resulting space groups [5,6]. Howard and Stokes [5] demonstrated that all the pure tilt transitions could be generated by the two representations $R_4^+$ and $M_3^+$ or a linear combination $R_4^+ \oplus M_3^+$. A recent summary of the structural and chemical variety of perovskites is given by Mitchell [7].

*Corresponding author. Fax: +1-613-584-4040.
*E-mail address:* ian.swainson@nrc.gc.ca (I.P. Swainson).

0022-4596/$ - see front matter 
doi:10.1016/S0022-4596(03)00352-9

Neither the RUM nor the group classification of possible tilt structures allows one to predict which of the many possible structures will form. However, there are methods that create a high degree of predictability of the tilt system on the basis of the large amount of crystal chemical information available for most perovskites with atomic cations [8,9]. Thomas has developed a system for predicting the degrees of tilt for certain tilt systems, based on geometrical arguments [10,11].

For systems such as MAPX the non-spherical symmetry of the *A*-cation brings in the possibility of extra transitions, due to orientational order–disorder phenomena. The cubic *Pm*3*m* phase is not compatible with an orientationally ordered *MA*-ion. It seems likely that any order–disorder phenomena of the cations will be strongly coupled to the potential transitions of the framework itself, since the framework defines the cage in which the *MA*-cation sits. The ordered, low-temperature phases could belong to a different space group from those found in the standard tilt systems, due to possible additional symmetry-breaking when the cation orders. Furthermore, because of the polar nature of the *MA*-ion, it allows an examination of the effects of hydrogen-bonding between the *MA*-cation and the framework itself. We note in passing that there is some debate in the case of crystalline ammonium compounds, that commonly show rotational disorder, whether these weak directional interactions between protons and the cages should in general be termed hydrogen bonds [12].

The MAPX were synthesized by Weber [13], who reported they were perovskites. Poglitsch and Weber [14] studied the phase transitions on cooling MAPX, and in the case of methylammonium lead bromide (MAPB) showed there existed four phases which they labelled $\alpha - \delta$, but which subsequent workers have generally referred to as I–IV. They suggested space groups on the basis of observed reflections and corresponding systematic absences in Guinier photographs. These space groups have generally been accepted by later workers and have, for instance, been the basis of the interpretation of infrared spectra and Landau models [15,16]. A recent overview of the complex structural chemistry of organometallic perovskite-related phases has been given by Mitzi [17].

The phase relations as a function of pressure (0–200 MPa) and temperature (100–380 K) have been reported by Onoda-Yamamuro et al. [18] who calculated $\Delta V$ for the transitions in each halide and performed calorimetric measurements on the transitions. NMR, calorimetry, and infrared spectroscopic were performed by Knop et al. [19] who examined the states of disorder for the phases of MAPX as a function of temperature. The transition temperatures for protonated material are I–II 235.1(2) K and II–III 154.2(2) K and III–IV 148.35(5) K [19].

## 2. Experimental

### 2.1. Sample preparation

Samples were prepared following well-described methods [13,19]. In the case of the neutron sample, N-deuterated MAPB was produced by using fully deuterated DBr (MSD Isotopes), and reactor grade (>99.8%) $D_2O$ (Atomic Energy of Canada Limited—AECL). The $D_2O$ was also used to deuterate all exchangeable hydrogens of the precursor chemicals prior to the final synthesis. A fine bright orange precipitate was formed which was filtered and transferred to a desiccating chamber prior to the diffraction measurements.

### 2.2. X-ray powder diffraction

As a preliminary to the neutron measurements, variable temperature X-ray diffraction measurements were performed from 120 K to room temperature on samples mounted in 0.1 mm diameter capillaries, mounted in an Enraf-Nonius Guinier-Simon camera, using Cu$K\alpha_1$ radiation. The temperatures were corrected from a calibration curve based on the melting points of several liquids and are probably accurate to between 3 and 5 K over the full temperature range.

All four phases of MAPB were observed and the transition temperatures estimated as 232(3), 156(3) and 146(3) K, in agreement with the calorimetric measurements [19]. The temperature dependence of the lattice parameters of phases III and IV could not be established from this method, and although a diffraction pattern of pure phase III was obtained, the higher order reflections were diffuse.

### 2.3. Neutron powder diffraction

Neutron powder diffraction was used to study the orientational order of the *MA*-ions within the cages of the low-temperature structure. X-rays are not particularly easy to use for this purpose as the signals are dominated by the scattering from Pb and the halides. Distinguishing C and N is far from trivial in such an environment and finding hydrogen atoms would be very unlikely. On the other hand, fully protonated samples would be difficult to study with neutrons due to the large amount of incoherent scattering. All the results presented in this paper come from the neutron refinements of the N-deuterated material. We prepared $CH_3ND_3PbBr_3$ in order to study this phenomenon. The N-deuterated sample reduced incoherent scattering to a manageable level, and this selective deuteration has the additional benefit of labelling one end of the *MA*-ion as a strong positive scatterer ($-ND_3$), while the other end ($-CH_3$) is terminated with negative scattering length protons.

The neutron powder diffraction measurement was performed on the C2 diffractometer at Chalk River Laboratories, Chalk River, Ontario. The diffractometer consists of an 800 wire $BF_3$ detector spanning 80° $2\theta$, $\Delta = 0.1°$ $2\theta$, which floats pneumatically over an epoxy dancefloor. The incident wavelength used for the Rietveld refinements of 1.32860(3) Å was calibrated with an external Si powder standard and obtained from a Si(531) reflection at ca. 92.7° take-off angle. For indexing runs the wavelength selected was 2.36869(3) Å from a Si(311) reflection at the same take-off angle. During the indexing runs the beam was filtered with a pyrolitic graphite filter (Panasonic Super Graphite). Data were collected and refined in two separate banks from 3–83° and 37–117° $2\theta$ with wire-spacing 0.1° over the temperature range of 11–250 K. Each bank was collected for 1 h. Data consisting only of background far below the first diffraction peak were removed from the fit of the first bank.

We indexed the diffraction pattern from phase IV using the CRYSFIRE suite [20] and found an orthorhombic basis with the same dimensions as that suggested by Poglitsch and Weber [14]. The basis is a little odd since in most orthorhombic perovskites the two "pseudo-tetragonal" axes, $a$ and $c$ in standard settings, differ by small amounts, whereas in this case they are significantly different in magnitude. One of the candidate space groups satisfying observed absences was $Pna2_1$ as previously suggested [14].

In order to begin the refinement we generated a starting model by using a technique we have used before for phase transitions in molecular solids, by treating the both the *MA*-ion and the $PbBr_6$ as rigid bodies (RBs) using the GSAS package [21]. The definition of the RB used for the *MA* ion is given in Table 1. The RBs are then placed into the lattice in an initially "random" orientation and allowed to refine orientation and, where applicable, shifts from projected centers-of-mass, with aninitially high degree of damping. The $PbBr_6$ were overspecified as independent octahedra with all 6 Br atoms defined with partial occupancies, and the connectivity between neighboring octahedra was not specified. The connectivity becomes generated as the orientations of the octahedra refine to optimize the fit to the observed pattern. As the orientations settled down, the $PbBr_6$ octahedra were replaced by an ordered atomistic model, which allowed for distortions of the octahedra. As a final step, the RB

Table 1
Refined structure of $CH_3ND_3PbBr_3$ in phase IV, space group *Pnma*, at 11 K. $a = 7.9434(4)$ Å, $b = 11.8499(5)$ Å, $c = 8.5918(4)$ Å

| Atom | $x$ | $y$ | $z$ | $U_i^*100$ (Å$^2$) | Site |
|---|---|---|---|---|---|
| N | 0.0481(6) | 0.25 | −0.0952(6) | 0.80(9) | $M$(010) |
| C | −0.0187(9) | 0.25 | 0.0650(7) | 0.80(9) | $M$(010) |
| H1 | 0.0279(14) | 0.3232(9) | 0.1245(11) | 1.89(12) | 1 |
| H2 | −0.1576(19) | 0.25 | 0.0484(18) | 1.89(12) | $M$(010) |
| D1 | 0.0081(9) | 0.3189(5) | −0.1568(6) | 1.89(12) | 1 |
| D2 | 0.1779(12) | 0.25 | −0.0954(10) | 1.89(12) | $M$(010) |
| Pb | 0 | 0 | 0.5 | 0.01(11) | −1 |
| Br1 | −0.0324(7) | 0.25 | −0.5182(7) | 0.35(9) | $M$(010) |
| Br2 | 0.2940(5) | 0.02878(31) | −0.2880(5) | 0.35(9) | 1 |

Basis vectors defining the rigid body for the *trans* configuration of the methylammonium ion, used in the initial stages of refinement. $\omega$ is the internal angle of the tetrahedron, $\cos^{-1}(-1/3)$

| | Vector 1 | | | Vector 2 | | | Vector 3 | | |
|---|---|---|---|---|---|---|---|---|---|
| | C–N = 1.48 Å | | | C–H = 1.08 Å | | | N–D = 1.03 Å | | |
| | $x$ | $y$ | $z$ | $x$ | $y$ | $z$ | $x$ | $y$ | $z$ |
| C | 0 | 0 | 1/2 | 0 | 0 | 0 | 0 | 0 | 0 |
| N | 0 | 0 | −1/2 | 0 | 0 | 0 | 0 | 0 | 0 |
| H | 0 | 0 | 1/2 | $\sin\omega$ | 0 | $\cos\omega$ | 0 | 0 | 0 |
| H | 0 | 0 | 1/2 | $-\sin\omega\cos 60°$ | $\sin\omega\sin 60°$ | $\cos\omega$ | 0 | 0 | 0 |
| H | 0 | 0 | 1/2 | $-\sin\omega\cos 60°$ | $-\sin\omega\sin 60°$ | $\cos\omega$ | 0 | 0 | 0 |
| D | 0 | 0 | −1/2 | 0 | 0 | 0 | $-\sin\omega$ | 0 | $-\cos\omega$ |
| D | 0 | 0 | −1/2 | 0 | 0 | 0 | $\sin\omega\cos 60°$ | $-\sin\omega\sin 60°$ | $-\cos\omega$ |
| D | 0 | 0 | −1/2 | 0 | 0 | 0 | $\sin\omega\cos 60°$ | $\sin\omega\sin 60°$ | $-\cos\omega$ |

Global values: $\chi^2 = 1.245$, $R_{wp} = 2.34\%$, $R_p = 1.81\%$, $R_{exp} = 2.10\%$, $n_{var} = 36$, $n_{obs} = 1540$.
*Low angle bank:* $R_{wp} = 2.36\%$, $R_p = 1.79\%$, $R_{exp} = 2.04\%$, $n_{obs} = 743$, $n_{hkl} = 452$.
*High angle bank:* $R_{wp} = 2.32\%$, $R_p = 1.82\%$, $R_{exp} = 2.20\%$, $n_{obs} = 797$, $n_{hkl} = 952$.

$$R_{wp} = \sqrt{\frac{\sum w(I_o - I_c)^2}{\sum wI_o^2}}, \quad R_p = \frac{\sum |I_o - I_c|}{\sum I_o}, \quad \chi^2 = \frac{\sum w(I_o - I_c)^2}{n_{obs} - n_{var}}.$$

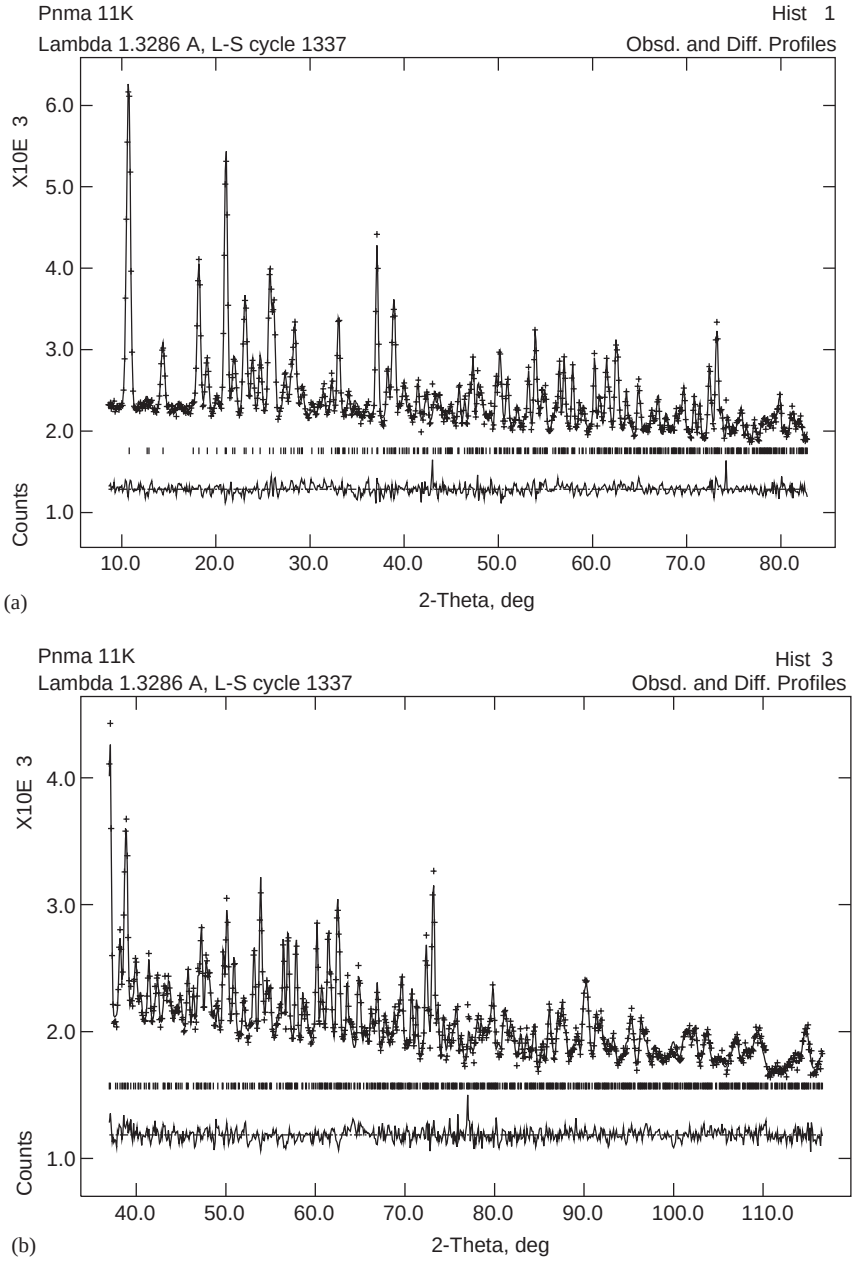


Fig. 1. Observed (crosses), fitted (lines) and difference (bottom) intensity of the powder pattern of MAPB at 11 K (a) low bank (b) high bank.

constraints on the *MA*-ion were released, leaving no geometrical constraints and damping was removed. The only constraints left were that all Br atoms were constrained to have the same atomic displacement factors, as were all H and D atoms. Observed, calculated and difference patterns are shown in Fig. 1.

## 3. Results and discussion

We examined the diffraction patterns from phase IV and using the previously suggested space group $Pna2_1$ [14] we obtained a satisfactory fit by mapping down the structure from the cubic phase. However, symmetry analysis with ADDSYM in PLATON [22] suggested there was missing symmetry and that the structure was centrosymmetric; the results were 100% *Pnma* with no unmatched atoms within the defaults of 1.00° (metric), 0.25 Å (distances) and 0.45 Å (inversion and translation), and a maximum deviation of 0.147 Å for a deuterium atom.

We transformed the $Pna2_1$ refinement to *Pnma* and obtained a good fit in this space group. Further checks showed no evidence for any other missed symmetry. The results of the refinement of MAPB in phase IV at 11 K are given in Table 1. Selected interatomic distances and angles are given in Table 2 and structure plots in Fig. 2. Classical hydrogen bonds were deduced

Table 2
Selected interatomic distances (Å) and angles (deg) for MAPB at 11 K. The notations $s_1$, $s_2$, $s_3$ correspond to the stalk lengths of the octahedron, and $\alpha_{xy}$, $\alpha_{xz}$, $\alpha_{yz}$ refer to their intersection angles [11]. These are used in the calculations in Table 3

| MA ion | | $PbBr_6$ octahedron | | $MABr_{12}$ cage distances | |
|---|---|---|---|---|---|
| N–C | 1.475(8) | Pb–Br1 ($s_3/2$) | 2.9770(6) | H1···Br3 (*2) | 2.916(12) |
| | | Pb–Br2 ($s_2/2$) | 2.982(4) | H2···Br1[a] | 2.989(17) |
| N–D1 (*2) | 1.023(6) | Pb–Br2 ($s_1/2$) | 2.986(4) | | |
| N–D2 | 1.031(10) | | | D1···Br2 (*2) | 2.525(7) |
| C–H1 (*2) | 1.073(12) | Br1–Pb–Br2 ($\alpha_{xz}$) | 83.2(1) | D2···Br1 | 2.500(11) |
| C–H2 | 1.112(17) | Br1–Pb–Br2 ($\alpha_{yz}$) | 89.2(1) | | |
| | | Br2–Pb–Br2 ($\alpha_{xy}$) | 84.83(3) | C–H1···Br2 (*2) | 165.0(9) |
| C–N–D1 (*2) | 111.8(5) | | | C–H2···Br1 | 177.7(11) |
| C–N–D2 | 111.2(7) | | | | |
| N–C–H1 (*2) | 108.7(7) | | | N–D1···Br2 (*2) | 151.2(6) |
| N–C–H2 | 103.8(9) | | | N–D2···Br1 | 156.9(8) |
| | | | | | |
| D1–N–D1 | 105.8(9) | | | | |
| D1–N–D2 (*2) | 108.0(6) | | | | |
| H1–C–H1 | 107.9(11) | | | | |
| H1–C–H2 (*2) | 113.8(7) | | | | |

[a] Not a hydrogen bond, according to the criteria of PLATON [19]. $d(H\cdots Acc) < r(H) + r(Acc) - 0.12$ Å; $d(Don\cdots Acc) < r(Don) + r(Acc) + 0.50$ Å; Don–H···Acc > 100°, where Don = donor, Acc = acceptor.

by PLATON [22] between the $ND_3$ group and Br atoms in different octahedra. The criteria used for the hydrogen bond calculation in PLATON [22] are $d(H\cdots Acc) < r(H) + r(Acc) - 0.12$ Å; $d(Don\cdots Acc) < r(Don) + r(Acc) + 0.50$ Å; Don–H···Acc > 100°, where Don stands for donor and Acc for acceptor. It also suggested that H1 of the methyl group was bonded to the Br cage, although if such an interaction exists, it will be very weak. Only H2 appears not to be hydrogen bonded, from these criteria (Fig. 2b). *Pnma* is one of the standard space groups of tilted perovskites with atomic cations, and the orientational ordering of the *MA*-ion is achieved without further symmetry-breaking. The C–N bond lies normal to the *b*-axis, and the C→N vector alternates around this axis (Fig. 2a). *Pnma* ($GdFeO_3$ structure) is the most common structure-type for simple perovskites and corresponds to the $a^-b^+a^-$ tilt system in the modified Glazer notation [23].

We note that head-to-tail rotational disorder of the *MA*-cation is fully removed in this phase, as previously suggested [18,19]. The H/D atoms are well-localized and the molecular cation is in a low-energy *trans* configuration, with the two H and two D atoms not on *m*(010) having a refined H1–C–N–D1 torsion angle of 179.44°, also suggesting negligible rotational disorder about the C–N axis. Knop et al. [19] demonstrated that C–N rotational disorder was the first form of disorder to commence on heating, on the basis of observations from D and $^{14}N$ NMR.

### 3.1. Relationship to the $Pna2_1$ cell

Poglitsch and Weber [14] had no structural information and only Guinier film on which to base their suggestion of $Pna2_1$ ($a \sim 7.97$ Å, $b \sim 8.58$ Å, $c \sim 11.85$ Å). It is easy to reconcile the suggestion of $Pna2_1$ with that of our refinement in *Pnma* as the systematic absences in a powder pattern are identical.

Historically, a similar situation existed with one of the phases of $PbZrO_3$ [11] and $NaTaO_3$. $NaTaO_3$ was originally placed in space group $Pc2_1n$ [$Pna2_1$] [24] before being ascribed to *Pcnm* [*Pnma*] [25]. Because of this, it would also appear likely that phase III of $CH_3NH_3PbI_3$, stable below ~145 K, currently classified as $Pna2_1$ [14], also has space group *Pnma*.

### 3.2. Nature of the distortion

Given that there are many potential soft structures, why should the ordered phase of MAPB choose this one? Lufaso and Woodward [23] have shown that *Pnma* is favored when the ionic tolerance factor is <0.98 or when an atomic *A* cation is relatively electronegative. While many pervoskite distortions are predictable for simple cations, this does not appear to be the case for perovskites with complex cations. An additional consideration here is that any possible structure in which the cation orientationally orders has to be able to accommodate the rather elongate shape of the *MA*-ion. However, the final structure is probably also driven by optimizing the hydrogen bonding between the guest and the potential cages offered by the various possible soft structures.

The geometry of the *MA*-cation is still very close to the RB-shape defined in the early stages of the refinement, the Pb–Br bond lengths are reasonably regular, and the two independent D···Br hydrogen bond lengths are also reasonably close. The largest distortions

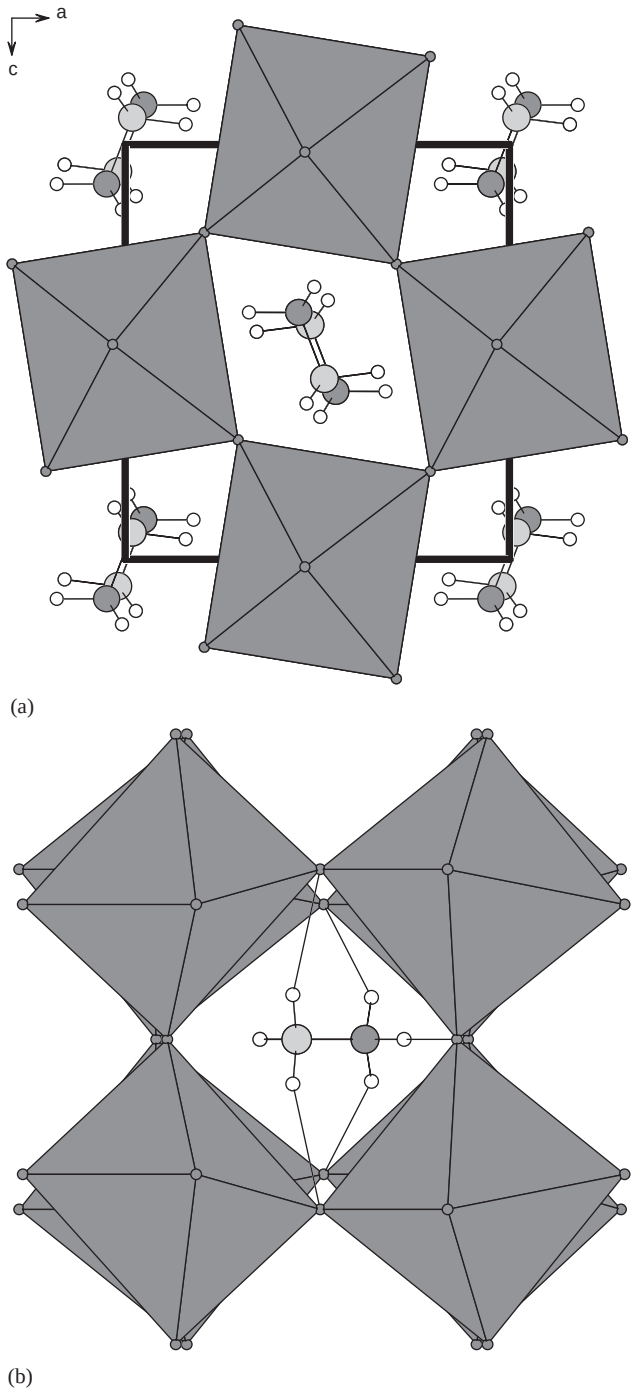


Fig. 2. View of structure (a) down $b$. The MA cation lies in 0 0 1, is *anti*-ordered up the $b$-axis and is displaced along approximately $\langle 110 \rangle_{Pnma}$ directions, (b) down $[10\bar{1}]$ showing the cage environment about a single $MA$ cation in the vicinity of (1/2, 1/4, 1/2) and the classical hydrogen bonds suggested by PLATON [22]. The shading scheme of the $MA$ cation is: C light-colored, N-dark colored, D/H transparent. H2 is the non-hydrogen-bonded hydrogen atom.

in the low-temperature structure are associated with the angular regularity of the $PbBr_6$ octahedron. This is reflected in the relatively large angular variance ($BAV_B$) and the reasonably regular quadratic elongation ($QE_B$), defined in Ref. [26], of the $BX_6$ octahedron (Table 3).

As *Pnma* can be generated by a pure tilt transition [5,6], the observed distortions of the $PbBr_6$ are not a symmetry requirement for transformation to this phase. Octahedral tilting values, as defined in Ref. [11], are shown in Table 3, calculated from the values presented in Tables 1 and 2. Here we modify the basis of Ref. [5] so that the $b$-axis of *Pnma* maps to the $c$-axis (rather than $b$) of $Pm3m$. The transformation matrix is therefore

$$\begin{pmatrix} a \\ b \\ c \end{pmatrix}_{Pnma} = \begin{pmatrix} 1 & 1 & 0 \\ 0 & 0 & 2 \\ -1 & 1 & 0 \end{pmatrix} \begin{pmatrix} a \\ b \\ c \end{pmatrix}_{Pm3m}.$$

The choice of which cubic axis to refer $b$ to is arbitrary but this choice is somewhat more consistent with the notation given in Ref. [11] of $\theta_m$ and $\theta_z$ in pseudo-cubic axes. $\theta_m$ is the mean tilting around $x$ and $y$ and $\theta_z$ that about $z$. Using this definition the unique $z$-axis is parallel to the $b$-axis of *Pnma*. The degree of tilt $\Phi$ is defined as $1-\cos^2\theta_m\cos\theta_z$ and the theoretical polyhedral volume ratios $V_A/V_B^t$ have the values [11]:

$V_A/V_B^t = 5$ characteristic of the undistorted phase,
$V_A/V_B^t = 5-6\Phi$ for a system with no internal distortion of the octahedra.

The observed polyhedral volume ratio is denoted $V_A/V_B^a$. Values of $V_B$ were calculated with the aid of IVTON [27] and checked with VOLCAL [28]. The value of $V_A$ can be most accurately calculated by the relation $V_A = V_U/Z - V_B$, where $Z$ is the number of formula unit per cell and $V_U$ the unit cell volume. For fluorides, oxides and hydrides $V_A/V_B^a$ and $V_A/V_B^t$ coincide to a few parts per mil or better. There are only five examples in the tabulation given in Ref. [11] that lie off the relationship between $\Phi$ and $V_A/V_B$, and all are associated with appreciable octahedral distortions as observed here. This is confirmed by $\Delta_{perp}$, defined as $1-\sin\alpha_{xy}\sin\alpha_{yz}\sin\alpha_{xz}$. The value calculated for MAPB is the largest, with the exception of $NaTaO_3$, when compared to the list of oxides and fluorides given in Ref. [11]. This is echoed in the large difference between $a$ and $c$ in both MAPB and $NaTaO_3$.

The tilts and octahedral distortions are probably arranged so that the $A$ cation is in an environment that optimizes the hydrogen bonding between cation and cage. In *Pnma* the $A$ cation is free to move in the $AX_{12}$ cage. The position of the $MA$ cation (as defined by the midpoint of the C–N bond) is 0.0147(11), 1/4, −0.0151(9), as opposed to its ideal location of 0, 1/4, 0. To within error, it is therefore displaced along a vector close to $(10\bar{1})$ *Pnma* or sub-parallel to one of the cell edges of the cubic phase, in the pseudo-tetragonal plane. This shortens the D···Br and extends the H···Br distances. The optimization of the hydrogen bonding

Table 3
Selected polyhedral tilts and distortions as defined by Thomas [11] for MAPB at 11 K

| | | | | | | | |
|---|---|---|---|---|---|---|---|
| $\theta_m$ | 11.350° | $V_B$ | 34.9556 Å$^3$ | $V_A$ | 167.226 Å$^3$ | $V_A/V_B^t$ | 4.737 |
| $\theta_z$ | 5.862° | $QE_B$ | 1.00738 | $\Delta_{perp}$ | 1.107e$^{-2}$ Å | $V_A/V_B^a$ | 4.784 |
| $\Phi$ | 0.0438 | $BAV_B$ | 26.502°$^2$ | $(s_1+s_2)^2/s_1s_2$ | 4.000 | $\Delta V_A/V_B$ | −0.047 |

therefore involves the interplay of several degrees of freedom: pure octahedral tilts inherent to the transition, octahedral distortion, cation displacement, and presumably molecular rotation of the cation in its *trans* configuration. There is only weak temperature dependence to phase IV. Neither the cage nor the orientation of the *MA* cation changes significantly: e.g., our refinements show that $\theta_m$ and $\theta_z$ are 10.33° and 5.55° at 138 K (cf. analysis from refinements of 11 K data in Table 3).

It is interesting to note that the low-temperature structure of $CD_3ND_3SnBr_3$ has been examined and observed to be rhombohedral [29]. Unfortunately, full structural details do not appear to have been published.

## 4. Relationship to the upper phases

We took neutron diffraction measurements from phase I to IV. Both neutron and X-ray measurements confirm that phase II, stable between 154.2 and 235.1 K [19] is of symmetry $I4/mcm$. We do not present a full refinement of the neutron data in phase II due to the difficulty of adequately modelling the intensity from the rotational disorder of the *MA* cation. Nevertheless we performed tests in which we placed a disordered *MA* RB in different orientations in phase II, and refined the $PbBr_6$ cage and thermal factors. We tested cases with the *MA*-axis parallel to ⟨001⟩, ⟨100⟩ and ⟨110⟩. There was only a small difference in the quality of the refinements where the *MA* ion was parallel to ⟨100⟩ and ⟨110⟩, but there was a discernible increase in $\chi^2$ in the ⟨001⟩ case. This strongly suggests the *MA* ion is disordered in the (001) plane, and together with the considerations of the magnitudes of $\Delta S_{I-II}$ [18] and the observations of electron densities in phase I [30], supports the conclusion that the preferred orientation of the *MA* ion may be ⟨110⟩ in the parent phase (model *DB* of Ref. [30]).

There is no group-subgroup relationship between *Pnma* and $I4/mcm$, so that it would be impossible to descend continuously through this sequence (see the possible transition pathways [5,6]). We did not observe phase III from the neutron data. Poglitsch and Weber [14] suggested it is $P4/mmm$, but this is not one of the space groups one could generate from pure tilt transitions [5,6]. It has also been demonstrated that single crystals in phase II of MAPC and phase III of MAPB [31] show additional reflections, which, in the case of MAPC at least, are due to an incommensurate distortion [31].

In the upper phases of MAPB it seems likely that the octahedral framework shows some degree of dynamic disorder. Certainly, there is evidence of a structured diffuse background in the diffraction patterns. This disorder appears to be a standard phenomenon in the high symmetry phases of frameworks in which RUMs are present, although the number of RUMs is much reduced in cubic perovskites compared to a system such as the open tetrahedral framework of $\beta$-cristobalite [32]. This disorder would fit the observation that the cell side of phase I for MAPX is less than the sum of the ionic radii [29] and that the refined anisotropic temperature factors from X-ray data show much larger values transverse to the bonds than normal to the bonds [19]. It seems likely that there is a strong coupling between these dynamic tilt fluctuations and the orientational disorder of the elongate *MA* cation. Tumbling about the C–N axis of MAPB is strongly reduced in phase II and stops completely in phase III [19].

A listing of the refined cell parameters as a function of temperature is shown in Table 4. The spontaneous strains in the lower phases are referred back to the cubic phase are shown as a function of temperature in Fig. 3. The definition of the strains $e_1(T)$ is

$$e_1(T) = \frac{a(T) - a_0(T)}{a_0(T)},$$

where $a(T)$ is the value of the cell edge referred back to cubic axes, and $a_0(T)$ the value extrapolated from phase I. $e_2$ and $e_3$ are similarly defined. One can see that the strains generated in phase IV are very large in comparison to those in phase II.

## 5. Conclusions

The space group of phase IV of MAPB is that of one of the standard tilt systems in perovskites: *Pnma*. This structure is therefore centrosymmetric, rather than polar as previously suggested. We suggest that the tilt system in the ordered phase is selected to conform to both the general elongate shape of the *MA*-cation and to optimize the hydrogen bonding between the guest and the cage. The $PbBr_6$ octahedron shows a deviation from angular regularity. It seems likely that the symmetry of

Table 4
Listing of refined lattice parameters of MAPB, versus temperature. Over the range 250–225 K MAPB was refined in *Pm*3*m*, 220–157 K, *I*4/*mcm*, and 145–11 K as *Pnma*

| *T* (K) | *a* (Å) | *b* (Å) | *c* (Å) |
|---|---|---|---|
| 11 | 7.9434(4) | 11.8499(5) | 8.5918(4) |
| 35 | 7.9452(4) | 11.8507(6) | 8.5906(4) |
| 60 | 7.9521(4) | 11.8516(6) | 8.5886(4) |
| 85 | 7.9658(4) | 11.8525(6) | 8.5841(4) |
| 110 | 7.9856(5) | 11.8534(7) | 8.5771(5) |
| 125 | 7.9984(7) | 11.8551(9) | 8.5742(7) |
| 138 | 8.0086(6) | 11.8572(7) | 8.5696(6) |
| 142 | 8.0123(6) | 11.8567(8) | 8.5690(6) |
| 145 | 8.0160(7) | 11.8573(8) | 8.5676(6) |
| 157 | 8.3053(3) | 11.9019(7) | |
| 160 | 8.3073(3) | 11.8995(7) | |
| 180 | 8.3178(3) | 11.8977(8) | |
| 200 | 8.3257(3) | 11.8919(8) | |
| 210 | 8.3341(3) | 11.8822(9) | |
| 220 | 8.3443(3) | 11.8834(9) | |
| 225 | 5.9112(5) | | |
| 230 | 5.9134(4) | | |
| 235 | 5.9146(4) | | |
| 240 | 5.9154(4) | | |
| 250 | 5.9170(4) | | |

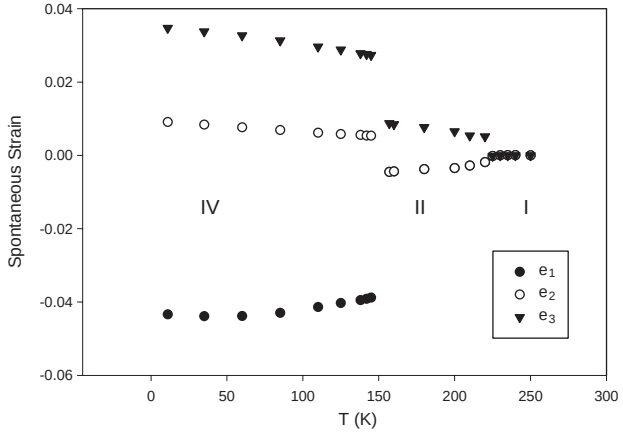


Fig. 3. Spontaneous strains $e_1$, $e_2$, $e_3$ as a function of temperature in phases I, II and IV.

phase III of the iodide will also be found to be *Pnma*, and that in phase II of MAPB, the *MA* ion is disordered in the tetragonal plane.

## References

[1] A.P. Giddy, M.T. Dove, G.S. Pawley, V. Heine, Acta Crystallogr. A 49 (1993) 697–703.
[2] K.D. Hammonds, A. Bosenick, M.T. Dove, V. Heine, Am. Mineral. 83 (1998) 476–479.
[3] A.M. Glazer, Acta Crystallogr. B 28 (1972) 3384–3392.
[4] A.M. Glazer, Acta Crystallogr. A 31 (1975) 756–762.
[5] C.J. Howard, H.T. Stokes, Acta Crystallogr. B 54 (1998) 782–784.
[6] K.S. Aleksandrov, J. Bartolomé, Phase Transit. 74 (2001) 255–335.
[7] R.H. Mitchell, Perovskites: Modern and Ancient, Almaz Press, Thunder Bay, ON, 2002.
[8] P.M. Woodward, Acta Crystallogr. B 53 (1997) 32–43.
[9] P.M. Woodward, Acta Crystallogr. B 53 (1997) 44–66.
[10] N.W. Thomas, Acta Crystallogr. B 45 (1989) 337–344.
[11] N.W. Thomas, Acta Crystallogr. B 52 (1996) 16–31.
[12] R.J.C. Brown, J. Mol. Struct. 345 (1995) 77–81.
[13] D. Weber, Z. Naturforsch. 33b (1978) 1443–1445.
[14] A. Poglitsch, D. Weber, J. Chem. Phys. 87 (1987) 6373–6378.
[15] A. Maalej, M. Bahri, Y. Abid, N. Jaïdane, Can. J. Phys. 77 (1999) 717–722.
[16] A. Maalej, Y. Abid, A. Kallel, A. Daoud, A. Lautie, Ann. Chim. Sci. Mater. 23 (1998) 241–246.
[17] D.B. Mitzi, J. Chem. Soc. Dalton Trans. (2001) 1–12.
[18] N. Onoda-Yamamuro, T. Matsuo, H. Suga, J. Phys. Chem. Solids 51 (1990) 1383–1395.
[19] O. Knop, R.E. Wasylishen, M.A. White, T.S. Cameron, M.J.M. Van Oort, Can. J. Chem. 68 (1990) 412–422.
[20] R. Shirley, CRYSFIRE Suite, The Lattice Press 41, Guildford Park Avenue, Guildford, Surrey, UK. 1999.
[21] A. Larson, R. Vondreele, GSAS: General Structure Analysis System, Los Alamos, NM, LAUR 86-748, 1986.
[22] A.L. Spek, PLATON—A Multi-Purpose Crystallographic Tool, Utrecht University, The Netherlands, 1999.
[23] M.W. Lufaso, P.M. Woodward, Acta Crystallogr. B 57 (2001) 725–738.
[24] H.F. Kay, J.L. Miles, Acta Crystalllogr. 10 (1957) 213–218.
[25] M. Ahtee, L. Unonius, Acta Crystallogr. A 33 (1977) 150–154.
[26] K. Robinson, G.V. Gibbs, P.H. Ribbe, Science 172 (1971) 567–570.
[27] T. Balić Žunić, I. Vicković, J. Appl. Crystallogr. 29 (1996) 305–306.
[28] L.W. Finger, VOLCAL, Carnegie Institute of Washington, Geophysical Laboratory, Washington, DC, USA, 1971.
[29] N. Onoda-Yamamuro, O. Yamamuro, T. Matsuo, H. Suga, K. Oikawa, N. Tsuchiya, T. Kamiyama, H. Asano, Physica B 213–214 (1995) 411–413.
[30] H. Mashiyama, Y. Kurihara, T. Azetsu, J. Korean Phys. Soc. 32 (1998) S156–S158.
[31] Y. Kawamura, H. Mashiyama, J. Korean Phys. Soc. 35 (1999) S1437–S1440.
[32] I.P. Swainson, M.T. Dove, Phys. Rev. Lett. 71 (1993) 193–196.